Catalysis Today 213 (2013) 18–24

Contents lists available at SciVerse ScienceDirect

Catalysis Today

journal homepage: www.elsevier.com/locate/cattod

Gas-phase conversion of 1,3-butanediol on single acid–base and Cu-promoted oxides

V.K. Díez, P.A. Torresi, P.J. Luggren, C.A. Ferretti, J.I. Di Cosimo*

Catalysis Science and Engineering Research Group (GICIC), INCAPE, UNL-CONICET, Santiago del Estero 2654, 3000 Santa Fe, Argentina

ARTICLE INFO

Article history:
Received 14 December 2012
Received in revised form 6 February 2013
Accepted 8 February 2013
Available online 18 April 2013

Keywords:
Dehydration
Dehydrogenation
Diols
Acid–base catalysis
Copper

ABSTRACT

The gas-phase conversion of 1,3-diols was studied on catalysts containing different active sites and using 1,3-butanediol as a model molecule. Transformation of the diol primary and/or secondary OH groups by dehydration and dehydrogenation reactions yields valuable oxygenates combining OH and C=C, OH and C=O or C=C and C=O functions, along with other compounds. A series of single oxides with different acid–base properties, copper–silica and copper-single oxide catalysts were prepared by several methods and characterized by TPR, XRD and N_2O chemisorption.

Acid–base oxides transform 1,3-butanediol at low rates. Oxide electronegativity determines the main reaction pathway: acidic oxides promote 1,3-butanediol dehydration toward unsaturated alcohols and olefins, whereas basic oxides dehydrogenate-dehydrate the diol toward the unsaturated ketone.

The effect of Cu^0 in monofunctional copper–silica, or bifunctional copper–acid or copper–base catalysts, is to increase the reaction rate and to shift the reaction pathway toward 1,3-butanediol dehydrogenation. The metal dispersion depends on the preparation method by impregnation, ion exchange or co-precipitation. Small Cu^0 particles strongly adsorb reactant and products allowing consecutive reactions to take place after initial dehydrogenation. In bifunctional catalysts, the role of the acid or base sites is to promote consecutive dehydration-hydrogenation or C—C bond cleavage reactions, respectively.

1. Introduction

Biomass-derived polyols such as glycerol, ethane-, propane- and butanediols present potential applications as natural organic building blocks. These C_2—C_4 molecules contain primary and/or secondary hydroxyl groups, and transformation of one in particular, or all the molecule OH groups can lead to other compounds used in organic synthesis.

Reactions like dehydration, dehydrogenation, or tandem dehydrogenation-dehydration-hydrogenation can convert polyols into valuable oxygenates such as unsaturated alcohols [1,2], furans [3], hydroxycarbonyl (aldol) compounds [4–7] and unsaturated carbonyl compounds [2,8], as well as into olefins [2] and other products. The product distribution will depend, among other factors, on the catalyst acid–base properties and on the presence or not of a metallic function in the catalyst formulation.

In particular, 1,3-butanediol (1,3-BDO), a C_4 diol containing one primary and one secondary hydroxyl group, can undergo dehydrogenation and dehydration reactions giving a variety of valuable compounds, grouped under different codes in Scheme 1. Aldol products (group HY, hydroxyketones and hydroxyaldehydes) combine OH and C=O functions as frequently required in pharmaceutical and food formulations, and in organic synthesis intermediates [9,10]; unsaturated alcohols (group UOL) are used in polymer industry, whereas saturated and unsaturated ketones (group K) are important intermediates for the synthesis of solvents, pesticides, terpenoids, as well as steroids, anticancer and other medical drugs [11].

In this work we present the results of the gas-phase conversion of 1,3-BDO on single oxides with different electronegativity. We report the effect of the oxide acid or base properties on the catalytic performance and on the reaction pathways.

Conversion of alcohols is known to proceed at higher rates on catalysts that contain a metallic function in addition to the acid or base site provided by the single oxide [12]. Thus, in order to investigate the role of a metallic site in the reaction, copper-containing catalysts were prepared by different methods and characterized by several techniques. Copper was chosen due to the known properties of this metal to preferentially activate the O—H bond of alcohols, giving aldehydes and ketones by dehydrogenation at mild temperatures without significant C—C bond cleavage. The effect of combining surface species (metallic and acid or base sites) was studied on a series of bifunctional copper-containing oxides prepared by incipient wetness impregnation and co-precipitation so that to vary the intimate contact between the metallic function and the acid or base site. Thus, the participation of Cu^0 sites in enhancing

* Corresponding author. Tel.: +54 342 4555279; fax: +54 342 4531068.
E-mail address: dicosimo@fiq.unl.edu.ar (J.I. Di Cosimo).

0920-5861/$ – see front matter © 2013 Elsevier B.V. All rights reserved.
http://dx.doi.org/10.1016/j.cattod.2013.02.030

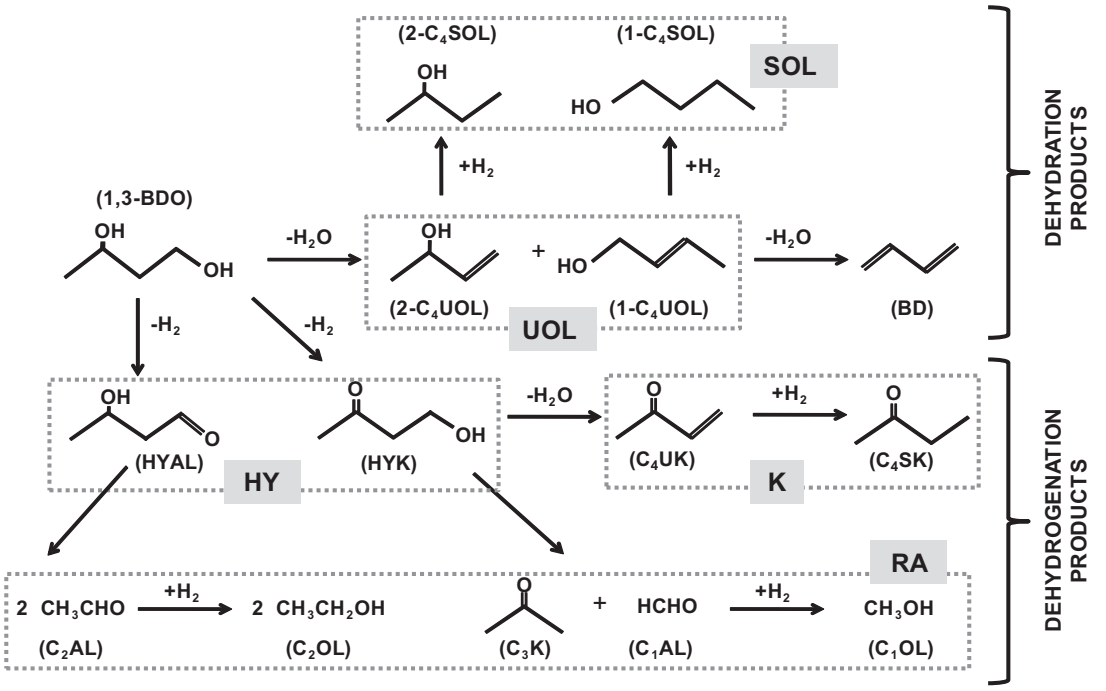

Scheme 1. Main reaction pathways for gas-phase 1,3-butanediol conversion.

the dehydrogenation performance was investigated in the presence of surface sites that promote other reactions. In addition, monofunctional silica-supported copper catalysts were prepared by ion exchange and incipient wetness impregnation. Catalytic tests with these samples were carried out to elucidate the influence of the copper particle size on the activity and selectivity.

2. Experimental

2.1. Catalyst synthesis and activation

Single oxides (M_yO_x) (MgO, Y_2O_3, CeO_2, Al_2O_3, TiO_2, ZrO_2, ZnO and Nb_2O_5) with different acid–base properties were prepared. High-surface area magnesium oxide was prepared by hydration with distilled water of low-surface area commercial MgO (Carlo Erba 99%; 27 m^2/g) and further decomposition of the resulting $Mg(OH)_2$ in a N_2 flow for 18 h at 773 K [13]. Y_2O_3 and CeO_2 precursors were prepared by precipitation method at a constant pH of 10. The precipitates were aged at 333 K, filtered, washed and dried at 348 K overnight [14]. The ZrO_2 precursor, i.e., $Zr(OH)_4$ was obtained by precipitation of zirconium oxychloride with ammonium hydroxide. All these precursors were decomposed in N_2 or air at 723–773 K overnight in order to obtain the corresponding oxides. ZnO was obtained by decomposition of commercial $(ZnCO_3)_2(Zn(OH)_2)_3$ (Anedra) in air at 623 K. Nb_2O_5 was prepared by decomposition at 773 K of commercial hydrated niobium pentoxide HY340 from Companhia Brasileira de Metalurgia e Mineracao (CBMM). Alumina and titania were commercial samples of γ-Al_2O_3 Cyanamid Ketjen CK 300 and TiO_2 P25 Degussa Hüls AG, respectively.

Cu-based catalysts containing 6–10 wt.% Cu were prepared by different methods. A silica-supported Cu catalyst (CuSi) was prepared by ion exchange (IE) through the so-called "chemisorption-hydrolysis" technique [15]. The solid was filtered, washed and dried overnight at 363 K. Finally, the solid calcined in air at 623 K during 5 h was denoted as CuSi-IE. Another CuSi sample was prepared by incipient wetness impregnation (I) [12]. After drying and calcination in air at 773 K, the sample was denoted as CuSi-I. Using similar procedures, CuAl-I and CuMg-I were prepared by impregnation of Al_2O_3 and MgO, respectively. In addition, catalyst precursors of Cu-containing CuM mixed oxides, where M = Mg^{2+} or Al^{3+}, were prepared by co-precipitation at a constant pH of 10 [12]. After filtering, washing and drying at 363 K, the precipitates were decomposed overnight in air at 723–773 K in order to obtain the corresponding mixed oxides. These catalysts were designated as CuMg-C and CuAl-C.

2.2. Catalyst characterization

BET surface areas (SA) were measured by N_2 physisorption at its boiling point using an Autosorb Quantachrome 1-C sorptometer. The sample structural properties were determined by X-ray Diffraction (XRD) technique using a Shimadzu XD-D1 instrument. The chemical content of Cu in all Cu-based catalysts was analyzed by Atomic Absorption Spectrometry (AAS).

Catalyst base site numbers (n_b) were measured by temperature-programmed desorption (TPD) of CO_2 preadsorbed at room temperature [14]. Samples were exposed to a flowing mixture of 3% of CO_2 in N_2 until surface saturation. Weakly adsorbed CO_2 was removed by flushing with N_2. Finally, the temperature was increased to 773 K at a ramp rate of 10 K/min. The desorbed CO_2 was converted into CH_4 on a Ni/Kieselghur catalyst at 673 K and then analyzed using a flame ionization detector (FID). Acid site numbers (n_a) were determined by TPD of NH_3. Samples were exposed to a 1.01% NH_3/He stream at room temperature until surface saturation. Weakly adsorbed NH_3 was removed by flushing with He. Temperature was then increased to 773 K at 10 K/min, and the NH_3 concentration in the effluent was measured by mass spectrometry (MS).

The dispersion of the metallic copper particles (D), defined as the ratio of the number of surface metallic copper atoms (Cu^S) to the total copper atoms (Cu^T) in the catalyst formulation, was determined by two consecutive experiments of temperature programmed reduction (TPR), using a reducing mixture of 5% H_2/Ar at a flow rate of 50 cm^3/min. Heating rates of 10 K/min from 298 to typically 653 K were used. A mass spectrometer (MS) in a Baltzers Omnistar unit monitored the hydrogen consumption. Thus, from

Table 1
Physicochemical properties of M_yO_x, CuSi, CuMg and CuAl catalysts and TOR values for copper-based catalysts.

Catalyst	χ_{oxide} [a] (Pauling unit)	Surface area, SA (m^2/g)	Cu loading (wt.%)	Structural analysis by XRD	Cu species reducibility and dispersion		TOR[g] (s^{-1})
				Phases detected	D[e] (%)	T_M[f] (K)	
MgO	2.12	192	–	Periclase	–	–	–
Y_2O_3	2.27	54	–	Bixbyite	–	–	–
CeO_2	2.37	75	–	Cerianite	–	–	–
ZnO	2.38	33	–	Wurtzite	–	–	–
ZrO_2	2.51	83	–	Tetragonal + monoclinic	–	–	–
Al_2O_3	2.54	230	–	γ-Alumina	–	–	–
TiO_2	2.63	54	–	Anatase + rutile	–	–	–
Nb_2O_5	2.73	84	–	Pseudo hexagonal	–	–	–
CuSi-I[b]	–	233	7.8	SiO_2 + CuO tenorite	4.3	527	1.18
CuSi-IE[c]	–	225	8.5	SiO_2	27.5	532	1.15
CuMg-I[b]	–	31	7.1	MgO	10.9	497	0.80
CuMg-C[d]	–	198	9.8	MgO	2.0	518	0.65
CuAl-I[b]	–	172	6.9	γ-Alumina	16·3	488	0·71
CuAl-C[d]	–	211	6.4	γ-Alumina	13·9	518	0·65

[a] Electronegativity.
[b] Prepared by impregnation.
[c] Prepared by ion exchange.
[d] Prepared by co-precipitation.
[e] Cu^0 dispersion by N_2O decomposition.
[f] Temperature at peak maximum by TPR.
[g] Mol 1,3-BDO/s mol surface Cu.

the first TPR experiment, the Cu^T value was obtained. The second TPR experiment was carried out after re-oxidation of the surface copper metal atoms to Cu_2O using N_2O and a stoichiometry of $Cu^S/N_2O = 2$ [16].

2.3. Catalytic testing

Vapor-phase conversion of 1,3-butanediol (1,3-BDO) was carried out at 523 K and 101.3 kPa in a fixed-bed reactor at contact times (W/F^0_{BDO}) of 0.2–33.0 g cat h/mol of 1,3-butanediol. Before the catalytic tests, catalysts were pretreated in a flow of N_2 at 623–773 K for 1 h. Then, the Cu-containing catalysts were reduced in situ in flowing H_2 (35 cm^3/min) at 573 K for 1 h. 1,3-BDO (Aldrich GC, 99.0%) was introduced via a syringe pump and vaporized into flowing N_2 (150 cm^3/min) to give a 1,3-BDO partial pressure of 2.3 kPa. Reaction products were analyzed by on-line gas chromatography using an Agilent 7890A chromatograph equipped with flame ionization detector and a 0.2% Carbowax 1500/80-100 Carbopack C packed column. Data were collected every 0.5 h for 5 h. Main reaction products were identified as 4-hydroxy-2-butanone (HYK), 2-butanone (C_4SK), 3-buten-2-one (C_4UK), acetaldehyde (C_2AL), methanol (C_1OL), ethanol (C_2OL), acetone (C_3K), 3-buten-2-ol (2-C_4UOL), 2-buten-1-ol (1-C_4UOL), 2-butanol (2-C_4SOL), 1-butanol (1-C_4SOL) and butadiene (BD). Due to a slight catalyst deactivation process, the catalytic results reported here were calculated by extrapolation of the reactant and product concentration curves to zero time on stream. Then, X, Y and S represent conversion, yield and selectivity at $t = 0$, respectively. Turnover (TOR) rates are defined as the moles of reactant converted per mol of copper surface site and per second.

3. Results and discussion

3.1. Effect of the catalyst acid–base properties on 1,3-BDO conversion reactions

Single oxides coded as M_yO_x were prepared and thoroughly characterized by several techniques. The textural and structural properties of these materials are given in Table 1. The M_yO_x materials are Lewis acids and the oxide electronegativities (χ_{oxide}) were calculated as the geometric mean of the atomic electronegativities using the Pauling's electronegativity scale. For an oxide with the formula M_yO_x, the bulk oxide electronegativity is [17]: $\chi_{oxide} = [(\chi_M)^y(\chi_O)^x]^{1/(y+x)}$. The surface acid ($n_a$) and base ($n_b$) site numbers of the M_yO_x catalysts were measured by integration of the NH_3 and CO_2 TPD curves (not shown), respectively [14]. Results plotted in Fig. 1 as a function of χ_{oxide} show that the n_b values (closed circles) decreased as the electronegativity increased, from 655 μmol/g on MgO to 7 μmol/g on Nb_2O_5. As expected for the Lewis acidity of the M_yO_x samples, the n_a values (open circles) roughly increased with increasing the oxide electronegativity.

The catalytic performance of the M_yO_x catalysts of Table 1 was investigated at 523 K and 101.3 kPa under kinetic conditions, i.e., at 1,3-BDO conversions (X_{BDO}) of ≈10%. The 1,3-BDO conversion rate (r_{BDO}, mmol/h g cat) values were plotted in Fig. 1 as a function of χ_{oxide} (open squares). The activity decreased with increasing the oxide electronegativity, suggesting that basic oxides are more active to convert 1,3-BDO. Thus, MgO was the most active M_yO_x catalyst of Table 1 with the exception of Al_2O_3, on which activity was fourfold higher compared to MgO. We found an analogous lack of correlation for alumina in the conversion of different monoalcohols on Lewis acid catalysts [12,18]. An explanation for this behavior might be the fact that the alumina used was a commercial sample

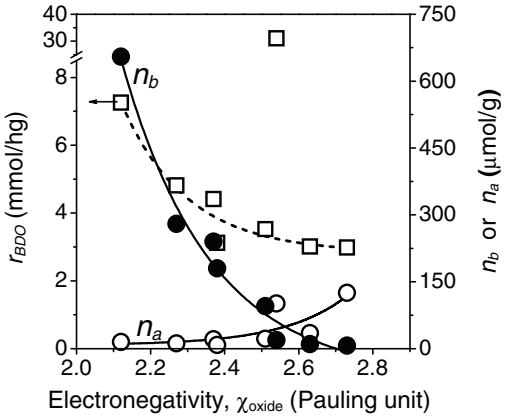

Fig. 1. 1,3-BDO conversion rate (r_{BDO}) and total acid (n_a) and base (n_b) site numbers as a function of the electronegativity of M_yO_x single oxides [T = 523 K; $\bar{P}_{BDO}$ = 2.33 kPa].

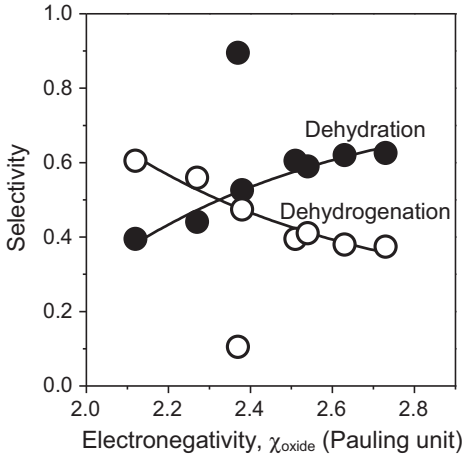

Fig. 2. Selectivity toward dehydrogenation and dehydration products on M_yO_x catalysts as a function of the electronegativity of M_yO_x single oxides [T = 523 K; $\tilde{P}_{BDO}$ = 2.33 kPa].

and may contain impurities. The superior performance of Al_2O_3 compared to other solid acids was also reported by Sato et al. [19] for the conversion of 1,3-BDO at much higher temperatures.

Since conversion of 1,3-BDO on acid–base catalysts gave a large number of products, we classified them in two major groups arising from initial dehydration and dehydrogenation reactions, Scheme 1. However, consecutive dehydration, hydrogenation and C—C bond cleavage reactions also took place. The reactant 1,3-BDO can undergo dehydration reactions leading to unsaturated alcohols (UOL) such as 3-buten-2-ol (2-C_4UOL) and 2-buten-1-ol (1-C_4UOL), which can be converted consecutively via hydrogenation or dehydration reactions, into saturated alcohols (SOL) or olefins (BD), respectively. Thus, the dehydration activity (r_{-H_2O}) includes UOL, SOL and BD formation. Similarly, 1,3-BDO can be transformed, via initial dehydrogenation, in hydroxycarbonyl compounds (HY) such as 4-hydroxy-2-butanone (HYK) and 3-hydroxybutanal (HYAL). Both HY compounds can undergo dehydration-hydrogenation to C_4 unsaturated and saturated ketones (group K) or decomposition by retro-aldol-like (RA) reactions giving C_1—C_3 alcohols, aldehydes and ketones. Therefore, dehydrogenation activity (r_{-H_2}) comprises formation of HY, RA and K compounds.

The effect of the M_yO_x surface acid and base properties on the dehydrating and dehydrogenating performance was investigated in Fig. 2, where the selectivities are plotted as a function of the oxide electronegativity. The dehydration selectivity, calculated as r_{-H_2O}/r_{BDO}, increased with increasing the oxide electronegativity whereas the dehydrogenation selectivity (r_{-H_2}/r_{BDO}) decreased. These results indicate that the main reaction pathway that takes place on basic oxides is 1,3-BDO dehydrogenation while acidic oxides predominantly dehydrate 1,3-BDO.

Although the activity of CeO_2 followed the general trend as a function of the electronegativity (Fig. 1), no correlation was found for the CeO_2 selectivity in Fig. 2. In spite of having a high number of basic sites, CeO_2 presents an enhanced dehydrating performance giving UOL in high selectivity. Sato et al. [19] obtained similar results when studied the dehydration of 1,3-diols on CeO_2 at higher temperatures (598 K) and attributed this behavior not to the weak acid–base properties but to the redox properties of this oxide. They postulated a radical dehydration mechanism with participation of Ce^{3+}–Ce^{4+} species in the catalytic cycle.

The distribution of dehydrogenation (r_i/r_{-H_2}; i = K, HY and RA) and dehydration (r_i/r_{-H_2O}; i = UOL, SOL and BD) products was studied in more detail in Fig. 3A and B, respectively. One of the most relevant features of Fig. 3A is that regardless of the acid–base properties, none of the oxides of Table 1 produced measurable amounts of the HY compounds. Although hydroxycarbonyl compounds (HYK and HYAL) are the primary products of the dehydrogenation pathway, Scheme 1, they were rapidly converted into K or RA products by dehydration or C—C bond cleavage reactions, respectively. The contribution of group K (saturated and unsaturated ketones) prevailed over that of RA and it was enhanced on more acidic oxides because K compounds are produced by dehydration of HY. The unsaturated ketone (3-buten-2-one, C_4UK) was the main constituent (85–95%) of group K because consecutive reduction of the C=C double bond of C_4UK toward 2-butanone (C_4SK) can proceed only if surface hydrogen fragments, resulting from 1,3-BDO dehydrogenation, are in the vicinity of the adsorbed C_4UK species. The contribution of short chain compounds (group RA), formed by retro-aldol-like reactions, was higher on basic oxides such as MgO and decreased with increasing χ_{oxide}. This result is somehow expected considering that gas-phase aldol condensation reactions are known to proceed at high rates on MgO and to a lesser extent on more acidic oxides [20].

On the other hand, Fig. 3B shows that, independently of the oxide electronegativity, UOL compounds were the main dehydration products on M_yO_x catalysts. The secondary alcohol (2-C_4UOL) predominated on CeO_2 but both UOL compounds depicted in Scheme 1 were obtained in similar concentrations on the rest of the M_yO_x oxides. The fact that 1,3-BDO elimination reactions proceed with high selectivities even on basic oxides is not surprising since in a previous work [21] we discussed that on strong solid bases, monoalcohols can undergo gas-phase water elimination by a E_{1cB} mechanism with formation of a C=C bond. A maximum was

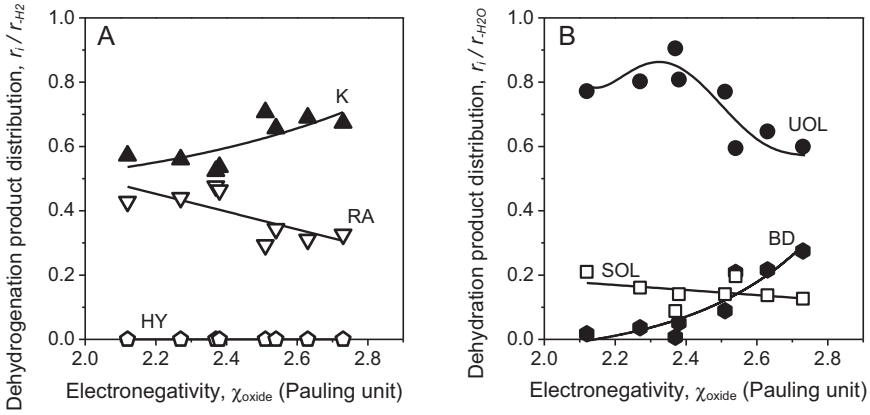

Fig. 3. Product distribution on M_yO_x catalysts as a function of the electronegativity of M_yO_x single oxides. (A) Dehydrogenation (i = K, RA and HY); (B) dehydration (i = UOL, SOL and BD) [T = 523 K; $\tilde{P}_{BDO}$ = 2.33 kPa].

observed in the UOL curve at about 2.4 due to the dehydrating properties of CeO_2, as explained above. On more electronegative oxides, consecutive dehydration of UOL toward olefins (BD) took place, thereby decreasing the UOL contribution. SOL formation by reduction of the C=C bond of UOL was not favored on any of the oxides; the slight decrease of the SOL curve is the consequence of the lower concentration of surface hydrogen fragments on more acidic oxides.

As a summary, 1,3-BDO can be transformed mainly by dehydration and tandem dehydrogenation-dehydration reaction pathways on acid–base catalysts, giving unsaturated alcohols and an unsaturated ketone, respectively. Hydroxycarbonyl compounds (HY) were completely converted to other products regardless of the acid or base character of the M_yO_x oxide.

3.2. Role of the metallic site in 1,3-BDO conversion

To investigate the effect of a metallic site on the gas-phase transformation of 1,3-BDO, two silica-supported copper catalysts (CuSi) with similar Cu loadings were prepared by different techniques. Silica was selected as a support because it does not present any measurable acidic or basic properties and therefore, the resulting materials can be considered as monofunctional metallic catalysts.

The physicochemical properties of the samples prepared by ion exchange (CuSi-IE) and impregnation (CuSi-I) are presented in Table 1. Analysis by XRD of unreduced catalysts, Fig. 4, showed a well defined CuO structure (tenorite) in CuSi-I, suggesting that in this sample CuO is present as large crystals. Contrarily, no crystalline CuO species could be detected in CuSi-IE, clearly indicating that the ion exchange technique gives rise to well dispersed CuO species. In agreement with these observations, whereas the Cu^0 dispersion was 27.5% in CuSi-IE, a 4.3% was measured in CuSi-I.

The results of the catalytic testing of CuSi samples are shown in Fig. 5, where CuO was included as reference. The metal dispersion in unsupported pure CuO was below the detection limit. Previously, a blank test using pure SiO_2 confirmed that the support was inactive for performing the 1,3-BDO transformations shown in Scheme 1. No acid or base site number could be measured on SiO_2. Furthermore, TPD of CO_2 carried out on CuSi samples indicated that these materials do not contain measurable amounts of base sites. Thus, CuSi-IE and CuSi-I catalysts present only a metallic function, the role of silica being to disperse Cu and to generate smaller Cu^0 particles than those of unsupported CuO.

A comparison between Figs. 1 and 5 indicates that CuSi catalysts were more active than the acid–base M_yO_x oxides to convert 1,3-BDO, given that r_{BDO} increased between 20- and 200-fold. As can be seen in Fig. 5, the order of catalytic activity (r_{BDO}) followed the order of the Cu^0 dispersion, i.e., CuSi-IE > CuSi-I > CuO. TOR values calculated for CuSi-IE ($1.15\ s^{-1}$) and CuSi-I ($1.18\ s^{-1}$) were quite similar, confirming that Cu^0 species are responsible for the catalytic activity of these samples.

Silica-supported copper catalysts and pure CuO convert 1,3-BDO to dehydrogenation products with more than 86% selectivity regardless of the metal dispersion. However, the distribution of dehydrogenation products (r_i/r_{-H_2}; i = K, HY and RA) changed depending on the metal dispersion. For instance, the HY group (black bars in Fig. 5) predominated on the large Cu^0 particles of pure CuO and gradually decreased from 0.64 to 0.47 and 0.37 on the smaller particles of CuSi-I and CuSi-IE. Only HYK was detected, thereby confirming the preferential dehydrogenation of the secondary OH function of 1,3-BDO. In contrast, as we explained above, no measurable amounts of HY compounds were detected on acid–base catalysts, Fig. 3A.

In a previous work we investigated the effect of copper loading on the dispersion and catalytic performance of silica-supported Cu catalysts [22]. We discussed there that HY compounds are

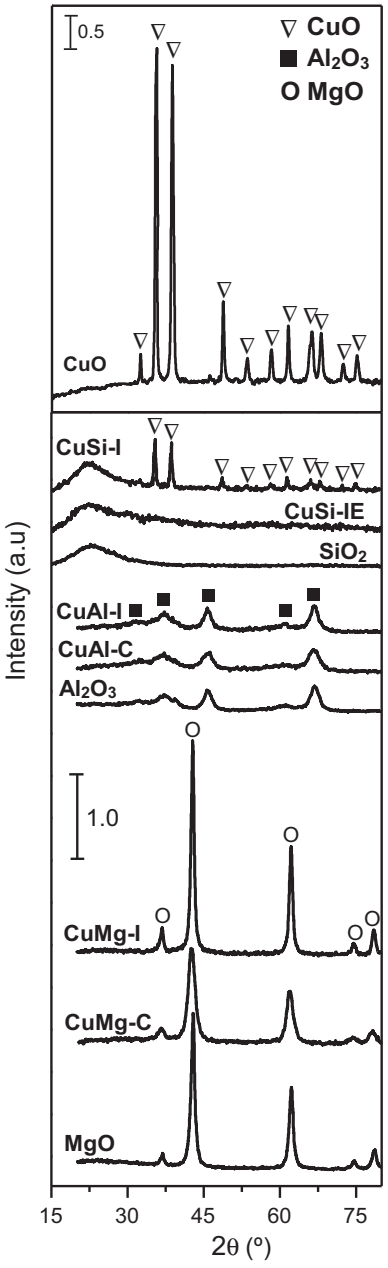

Fig. 4. XRD patterns of CuSi and CuM catalysts prepared by different techniques. Al_2O_3, MgO, SiO_2 and CuO included as reference.

unstable under gas-phase reactions conditions. They tend to react by dehydration or C—C bond cleavage reactions on highly dispersed Cu^0 particles due to a strong HY-copper site interaction. Therefore, on pure CuO, a weaker HY adsorption on large Cu^0 crystals would allow the release of HY to the gas phase before being converted in consecutive reactions, yielding HY in high selectivity. Contrarily, the strong HY adsorption on small metal particles allowed consecutive dehydration-hydrogenation reactions to take place. Thus, compounds of group K (white bars in Fig. 5), and particularly the saturated ketone C_4SK, were the main dehydrogenation products on the highly dispersed Cu^0 particles of sample CuSi-IE.

On the other hand, Fig. 5 also shows that RA compounds represent less than 20% of the dehydrogenation products and that their formation from HY seems not to be affected by the metal dispersion.

In conclusion, CuSi catalysts dehydrogenated 1,3-BDO at high rates. Activity and dehydrogenation product distribution depended

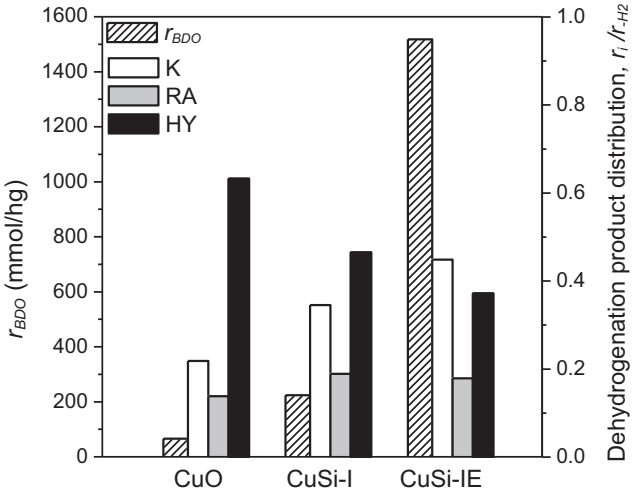

Fig. 5. 1,3-BDO conversion rate (r_{BDO}) and dehydrogenation product distribution (r_i/r_{-H_2}; i = K, RA and HY) on monofunctional CuSi catalysts prepared by different techniques. CuO included as reference [T = 523 K; $\bar{P}_{BDO} = 2.33$ kPa].

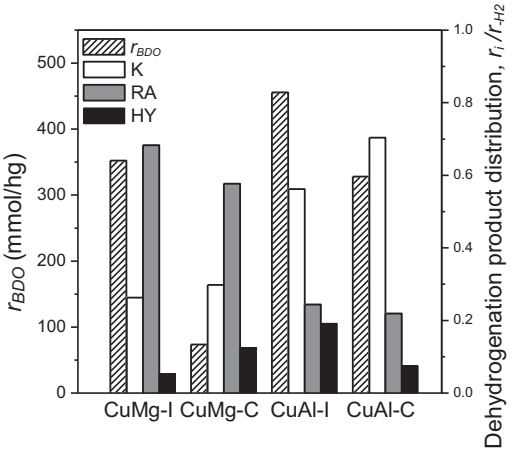

Fig. 6. 1,3-BDO conversion rate (r_{BDO}) and dehydrogenation product distribution (r_i/r_{-H_2}; i = K, RA and HY) on bifunctional CuM (M = Mg or Al) catalysts prepared by different techniques [T = 523 K; $\bar{P}_{BDO} = 2.33$ kPa].

on the dispersion of the Cu^0 particles. Ketones (HYK and C_4SK) resulting from the initial dehydrogenation of the secondary OH group of 1,3-BDO were the main products, with the hydroxyketone (HYK) being converted to the saturated ketone C_4SK on catalysts with a higher Cu^0 dispersion.

3.3. 1,3-BDO conversion on bifunctional CuM catalysts

CuM catalysts with M being Mg or Al were prepared to represent typically, bifunctional metal-base or metal-acid catalysts, respectively. Catalysts with similar copper loadings, prepared by incipient wetness impregnation of MgO or Al_2O_3 and by co-precipitation, were denoted as CuM-I and CuM-C, respectively. The physicochemical properties of these materials are shown in Table 1. The CuM-I samples presented lower surface area than the supports, probably due to a partial pore blockage by copper species during the impregnation procedure. The XRD patterns collected for unreduced CuM samples showed broad lines for CuAl samples (Fig. 4) corresponding to quasi-amorphous alumina. On the other hand, CuMg samples showed only the diffraction signal of MgO. Since no crystalline copper phase was detected, copper species in CuM catalysts were either highly dispersed on the surface forming amorphous domains not detectable by XRD or remained closely associated with the oxide structure after calcination. To investigate the copper-support degree of interaction and to elucidate whether copper causes a surface or a structural promotion in CuM oxides, additional TPR and metal dispersion measurement experiments were carried out.

The TPR studies showed that CuAl-I and CuAl-C catalysts completely reduced giving a single reduction peak at ≈490–520 K, indicating that copper is spread on the surface forming CuO species. In agreement with that, moderately high metal dispersions were measured on these samples, Table 1.

Contrarily, the TPR profiles of CuMg catalysts showed broad and asymmetric reduction peaks. In addition, just 33–40% of the total copper ions reduced in these samples, suggesting a strong Cu-Mg interaction that decreased the sample reducibility and cannot be assigned to a surface species because these samples were not fully reduced even at 1100 K. Thus, part of the Cu^{2+} ions seems to be in intimate contact with the MgO matrix giving rise to a non-reducible mixed oxide. In line with these findings, broad diffraction lines (Fig. 4) and a loss of crystallinity respect to pure MgO were observed for these samples (79% for CuMg-C and 88% for CuMg-I). These effects are likely caused by substitution of Cu^{2+} for Mg^{2+} ions within the periclase structure. Calculations of the lattice constant (a) for MgO (a = 4.214 Å), CuMg-I (a = 4.222 Å) and CuMg-C (a = 4.246 Å) showing the expansion of the MgO lattice in CuMg oxides, confirmed this assumption since the ionic radius of octahedrally coordinated Cu^{2+} ($r_{Cu^{2+}}$ = 0.73 Å) is slightly larger than that of Mg^{2+} in MgO ($r_{Mg^{2+}}$ = 0.72 Å) [23]. As a result, the Cu^0 dispersions were much lower than in the CuAl catalysts (2.0% in CuMg-C and 10.9% in CuMg-I). Similar low reduction degree has been observed also for Cu/MgO catalysts prepared by other techniques, but authors attributed this effect to a high Cu dispersion [24].

The catalytic performance of the CuM catalysts is presented in Fig. 6. The r_{BDO} values measured on bifunctional CuM catalysts were ≈10–50 times higher than on MgO and Al_2O_3 oxides (Fig. 1) and rather similar to the values on CuSi catalysts (Fig. 5). The improved activity of the CuM catalysts is the consequence of the ability of the Cu^0 atoms to promote the O—H bond cleavage in 1,3-BDO, leading to a remarkable shift of the reaction pathway toward dehydrogenation reactions, regardless of the acid or base nature of the support. Thus, Cu in CuMg enhanced the dehydrogenating properties of MgO increasing r_{-H_2}/r_{BDO} from 0.60 to ≈0.85. Also, Cu in CuAl worsened the dehydrating performance of alumina, from a r_{-H_2O}/r_{BDO} value of 0.59 to ≈0.15.

Since the presence of Cu^0 surface species accounts for the enhanced activity of CuM catalysts compared to single oxides, catalysts prepared by impregnation (CuMg-I and CuAl-I) were more active than their homologous prepared by co-precipitation (CuMg-C and CuAl-C), Fig. 6, because of a better copper reducibility and dispersion, Table 1. The similar TOR values measured for all the CuM samples, Table 1, confirm the participation of Cu^0 species in kinetically relevant reaction steps.

On CuAl-I and CuAl-C, compounds of group K were the main dehydrogenation products (Fig. 6), the majority being the saturated ketone (C_4SK). The slight differences between CuAl-I and CuAl-C regarding the dehydrogenation product distribution reflect the somewhat lower metal dispersion of the co-precipitated sample, in which the more exposed alumina sites interact more strongly with HY compounds forming K products. This clearly shows the role of the acid sites provided by alumina in dehydrating the HY compounds formed by initial 1,3-BDO dehydrogenation on CuAl catalysts.

The differences between CuMg-I and CuMg-C are noteworthy in terms of activity (r_{BDO}) since in the latter, copper ions are more occluded in the MgO matrix. In these catalysts with poorly or moderately dispersed Cu^0 species, the effect of the basic properties of

MgO is evident in the dehydrogenation product distribution. Both CuMg samples decomposed the HY compounds yielding products of group RA in high selectivity ($r_{RA}/r_{-H_2} = 0.58 - 0.68$). The strong adsorption of HY compounds on the MgO surface sites caused the C—C bond cleavage in the 1,3-BDO molecule, giving short chain oxygenates similarly to what was discussed above for pure MgO.

The studies carried out with bifunctional CuM catalysts lead us to conclude that Cu^0 surface sites initially dehydrogenated 1,3-BDO at high rates. The final dehydrogenation product distribution depended on the copper dispersion and on the acid or base nature of the accompanying cation M. On the other hand, UOL could not be obtained with CuM catalysts because the initial 1,3-BDO dehydration pathway is inhibited.

4. Conclusions

Biomass-derived 1,3-diols such as 1,3-butanediol can be converted into valuable oxygenates by dehydration or dehydrogenation reactions. Activity and product distribution are strongly dependent on the catalyst properties.

Single oxides with acid or base properties give unsaturated alcohols by dehydration at the primary and secondary OH groups. They also completely transform the initial 1,3-butanediol dehydrogenation product, a hydroxyketone (4-hydroxy-2-butanone), into an unsaturated ketone (3-buten-2-one) after consecutive dehydration, regardless of the acid or base character of the oxide. Surface base sites, on the other hand, favor the C—C bond cleavage leading the aldehydes, alcohols and ketones with lower carbon atom number.

Bifunctional copper–acid or copper–base catalysts convert 1,3-butanediol at much higher rates compared to single oxides. The enhanced activity is assigned to the ability of Cu^0 atoms to promote the O—H bond cleavage, shifting the reaction pathway toward dehydrogenation reactions. Thus, catalysts prepared by impregnation are more active than the co-precipitated counterparts because of a better Cu^0 particle dispersion. The dehydrogenation product distribution depends on both, the copper dispersion and the acid–base properties of the support. Thus, copper–Al_2O_3 gives mainly the hydroxyketone and the saturated ketone (2-butanone), but in addition to those products, copper–MgO forms products of lower carbon atom number. Studies on monofunctional Cu-SiO_2 catalysts indicate that the Cu^0 dispersion plays a major role in determining the final dehydrogenation product: the hydroxyketone is inevitably converted to the saturated ketone on highly dispersed Cu^0 species because of a stronger hydroxyketone-surface site interaction.

Acknowledgements

Authors thank the Agencia Nacional de Promoción Científica y Tecnológica (ANPCyT), Argentina (Grant PICT 1888/10), CONICET, Argentina (Grant PIP 11220090100203/10) and Universidad Nacional del Litoral, Santa Fe, Argentina (Grant CAID 51-248/09) for the financial support of this work.

References

[1] Y. Liu, H. Tuysuz, C.-J. Jia, M. Schwickardi, R. Rinaldi, A-H. Lu, W. Schmidt, F. Schuth, Chemical Communications 46 (2010) 1238–1240.
[2] N. Ichikawa, S. Sato, R. Takahashi, T. Sodesawa, Journal of Molecular Catalysis A: Chemical 256 (2006) 106–112.
[3] N. Ichikawa, S. Sato, R. Takahashi, T. Sodesawa, K. Inui, Journal of Molecular Catalysis A: Chemical 212 (2004) 197–203.
[4] S. Sato, M. Akiyama, R. Takahashi, T. Hara, K. Inui, M. Yokota, Applied Catalysis A: General 347 (2008) 186–191.
[5] C.-W. Chiu, M.A. Dasari, G.J. Suppes, AIChE Journal 52 (10) (2006) 3543–3548.
[6] S. Sato, R. Takahashi, T. Sodesawa, H. Fukuda, T. Sekine, E. Tsukuda, Catalysis Communications 6 (2005) 607–610.
[7] S. Sato, R. Takahashi, H. Fukuda, K. Inui, Journal of Molecular Catalysis A: Chemical 272 (2007) 164–168.
[8] A. Corma, G.W. Huber, L. Sauvanaud, P. O'Connor, Journal of Catalysis 257 (2008) 163–171.
[9] H. Zhang, G.T. Lountos, C.B. Ching, R. Jiang, Applied Microbiology and Biotechnology 88 (2010) 117–124.
[10] Y. Su, Y.-M. Liu, L.-C. Wang, M. Chen, Y. Cao, W.-L. Dai, H.-Y. He, K.-N. Fan, Applied Catalysis A: General 315 (2006) 91–100.
[11] N. Ichikawa, S. Sato, R. Takahashi, T. Sodesawa, Catalysis Communications 6 (2005) 19–22.
[12] J.I. Di Cosimo, G. Torres, C.R. Apesteguía, Journal of Catalysis 208 (2002) 114–123.
[13] J.I. Di Cosimo, V.K. Díez, C.R. Apesteguía, Applied Catalysis A: General 13 (1996) 149–166.
[14] C.A. Ferretti, A. Soldano, C.R. Apesteguia, J.I. Di Cosimo, Chemical Engineering Journal 161 (2010) 346–354.
[15] F. Boccuzzi, S. Coluccia, G. Martra, N. Ravasio, Journal of Catalysis 184 (1999) 316–326.
[16] E.D. Guerreiro, O.F. Gorriz, J.B. Rivarola, L.A. Arrúa, Applied Catalysis A: General 165 (1997) 259–271.
[17] R.T. Sanderson, Chemical Bonds and Bond Energy, 2nd ed., Academic Press, New York, 1976.
[18] J.I. Di Cosimo, V.K. Díez, M. Xu, E. Iglesia, C.R. Apesteguía, Journal of Catalysis 78 (1998) 499–510.
[19] S. Sato, R. Takahashi, T. Sodesawa, N. Honda, H. Shimizu, Catal. Comm. 4 (2003) 77–81.
[20] J.I. Di Cosimo, V.K. Díez, C.R. Apesteguía, Applied Clay Science 13 (1998) 433–449.
[21] V.K. Díez, C.R. Apesteguía, J.I. Di Cosimo, Catalysis Today 63 (2000) 53–62.
[22] P.A.Torresi, V.K. Díez, P.J. Luggren, J.I. Di Cosimo, Appl. Catal. A: General, (2013), in press, http://dx.doi.org/10.1016/j.apcata.2013.03.031
[23] http://abulafia.mt.ic.ac.uk
[24] S. Goodarznia, K.J. Smith, J. Molec. Catal. A: Chemical 353/354 (2012) 58–66.